Stress Distribution in the Western India-Eurasia Collision Zone: its Kinematics and Seismotectonic implications.

R. Arun Prasath*, Brijesh K. Bansal, Mithila Verma

Seismology/Geosciences, Ministry of Earth Sciences, Prithvi Bhavan, Lodhi Road, New Delhi, India.

*devanthran@hotmail.com | aprasath@es.iitr.ac.in

Keywords:

India-Eurasia Collision Zone; Stress Distribution; Garhwal-Kumaun Himalaya; Kashmir Earthquake; Karakoram Fault; Kaurik Chango Rift

Abstract: To evaluate stress distribution of the western India-Eurasia collision zone (IECZ), an iterative joint stress inversion technique has been applied to a declustered catalogue of 324 focal mechanisms for the first time. The results are then used to understand fault kinematics, seismogenesis and seismotectonics of the region. The inversion results reveal an NNE-SSW trending principal stress (σ1) with compression for the Himalayan seismic belt and an NNE-SSW trending σ1 with strike-slip stress regime for the Karakoram-Tibet, consistent with plate motion of the Indian plate. Within the Himalaya region, the western Himalaya (75º-77º E) exhibits arc-oblique compression (NE-SW) in contrast to arc-normal compression (NNE-SSW) in central Himalaya beyond 77°E; consistent with GPS vectors. Stress field for the aftershock sequence of the 2005 Kashmir earthquake in the Hazara Syntaxis region show dissimilarity with its surrounding regions (Pamir, Nanga Parbat, Hindukush, etc.), however, exhibits similarity with that of the Central Himalaya; therefore, we suggest this earthquake be Himalayan-type. Within the Karakoram-Tibet region, the Karakoram fault exhibits transpression oriented towards NNE-SSW, while the transverse structure i.e., the Kaurik Chango rift (KCR) located south of the Karakoram Fault shows transtensional motion with N-S oriented principal stress. The stress ratio in the western IECZ largely varies between 0.07 and 0.9, thus supports the significant role of the intermediate stress axis (σ2) in the areas of low-stress ratios. Besides, the low-stress ratios for Hazara Syntaxis, Karakoram-Tibet and KCR reveal the role of local structural variability and multiple tectonic forces suggesting heterogeneous stress field in the western IECZ.

Introduction

In general, earthquakes are caused by failure on critically stressed faults within the seismogenic layer of the crust (Wallace, 1951; Bott, 1959; Vavryčuk et al., 2015). Imaging the crustal stress field of an active region, using double-couple earthquake focal mechanism (FM) solutions could provide crucial information to understand the tectonic stress regime, its variability, and the role of local, regional, and transverse tectonics in earthquake generation. Knowledge of the stress regime would eventually help in constraining the kinematics, seismotectonics and seismic hazard estimation of a region. In the present study, the western part of the India-Eurasia Collision Zone (IECZ), predominantly compressional in nature, has been studied for imaging the stress field and its variability. The western IECZ is one of the ideal locations that ably represent the complex nature of structure and tectonics of IECZ that comprises of Himalayan intra-crustal boundary thrusts, normal faults in the Tethyan-Tibetan region and numerous transverse structures across the IECZ (Baranowski et al., 1984; Tapponnier et al., 1981). The western IECZ has experienced many destructive earthquakes in the past, such as M_w 7.6 Kashmir earthquake in 2005 (hereafter Kashmir earthquake) owing to the on-going plate convergence of 37-44mm/yr. between India and Eurasia continental plates (Banerjee and Bürgmann, 2002; Verma and Bansal, 2013 and references therein). Although the large/great earthquakes occur in the Himalayan front along the basal detachment, the majority of inter-seismic activity follow a linear trend, parallel to the Himalayan Arc, known as Himalayan Seismic Belt (HSB). The HSB is located between two intra-crustal boundary faults; Main Central Thrust (MCT) and Main Boundary Thrust (MBT). Besides these faults, two other major structures in the Tibetan Plateau of the western IECZ, namely, Karakoram Fault (KF) and Kaurik Chango

Rift (KCR) also show inter-seismic deformation through small to moderate size earthquakes (Gahalaut & Kundu, 2012; Ni & Barazangi, 1984).

A few earlier studies have attempted to image the stress field of western IECZ utilizing the available FM solutions for small areas (Gahalaut & Rao, 2009; Mahesh et al., 2015; Prasath et al., 2017; Yadav et al., 2016; Yadav et al., 2017). Mahesh et al. (2015) have used sufficient number of FM solutions for the Garhwal-Kumaun Himalaya, however, some of their solutions were for the earthquakes of magnitudes $M<2.0$, which raise concerns on the reliability of these solutions and the resultant stress field. Later, Prasath et al. (2017) obtained Moment Tensor (MT) solutions of earthquakes with magnitudes $3.0\leq M\leq 5.0$ which had good signal to noise ratios and estimated the stress field for the Garhwal Himalaya. However, this study did not include the events located outside their network. For Kinnaur-Chamba region, Yadav et al. (2016, 2017) obtained the stress field using a catalogue of FM solutions, compiled from various sources and some of their own solutions. While their own solutions are well constrained, some of the solutions of earlier studies, which were reported as slip and slip directions instead of strike, dip, and rake, had to be converted before stress inversions; these FM solutions were found erroneous. The study by Gahalaut and Rao (2009) has estimated the principal stress orientations for the earthquakes of the epicentral region of Kashmir earthquake (Hazara Syntaxial Zone) and reported a different stress field from the Himalaya, which raised concerns over this earthquake being a Himalayan-type earthquake. None of the above-mentioned studies applied declustering techniques to the catalogue used, therefore possibility of internal stress perturbations in their data and corresponding results cannot be ruled out. Considering these factors, imaging the current stress field with a comprehensive, robust and declustered catalogue attains importance for this region. Therefore, in this study, we utilized a declustered catalogue

of 324 reliable FM solutions with magnitudes 2.0≤M≤7.6 (from ~450 initial FM solutions) **to** image the crustal stress field, its variability and to understand the seismotectonics, fault mechanics and dominant tectonic forces acting on this part of the collision zone. Further, the new data and detailed analysis for the Hazara Syntaxial zone including the aftershock sequence of the Kashmir earthquake may help in comparing the stress regime with other parts of the Himalaya and its surroundings.

2. Structural setting

The structural setting of the western IECZ (29°-37°N latitudes and 72°-81°E longitudes), is highly complex and comprises the western Himalayan Syntaxial zone, Western Himalaya, Garhwal-Kumaun Himalaya and part of the southern Tibetan region (Figure 1 and 2). The Himalayan wedge (of both western and Garhwal-Kumaun Himalaya), sandwiched between southern Tibet in the north and the Indo-Gangetic plains in the south, occupies majority of the study area that comprises major intra-crustal boundary faults of the Himalaya, viz., Himalayan Frontal Thrust (HFT), MBT, MCT (locally known as Panjal Thrust), Southern Tibetan Detachment (STD) and Indus Tsangpo Suture Zone (ITSZ) (Figure 2) (Gansser, 1964). These northward dipping structures divide the region into four litho-tectonic units, namely, Sub Himalaya (SH), Lesser Himalaya (LH), Higher Himalayan Crystallines (HHC) and Tethyan Himalaya (TH) (Figure 2) (Gansser, 1964). Other distinct structural features in the Himalayan wedge are the Kishtwar Window (KW), Chamba Nappe (CN), Kullu-Larji-Rampur Window (KLRW) and Almora Klippen (AK) (Figure 2).

The Western Himalayan Syntaxial zone that occupies the northwestern part of the study area, comprises of Salt Range Thrust (SRT, western extension of HFT), Khairabad Thrust (KT,

western extension of MCT), Main Mantle Thrust (MMT, an extension of ITSZ) and Main Karakoram Thrust (MKT). This also includes Nanga Parbat Syntaxis (NPS) in its northwest and Hazara Syntaxial zone (HSZ) in its core, where the Kashmir earthquake had occurred. The other significant geological features in this part are Balakot Bagh Fault (BBF), Jhelum Fault (JF) and Kashmir Basin (KB), which demonstrate low seismic activity (Figure 3).

The major faults of the Himalayan arc emerge from a shallow and north dipping basal detachment fault, i.e., the Main Himalayan Thrust (MHT), located between varying depths of up to 20 km beneath the region (Ni &Barazangi, 1984). The locked portion of the MHT, where the majority of the ongoing convergence and deformation is taking place is estimated to be 100-120 km in width for the western and central Himalaya, whereas the syntaxial zone has broader width of 140-180 km (Li et al., 2018 and references therein).

Northeastern part of the study area composed of Karakoram and southern Tibet, which is mainly controlled by the structures such as, KF, MKT, MMT and KCR. The KF, a dextral fault of ~800 km length and divides the Tibetan plateau into two parts as northwest and southeast with varying slip rates (Leech, 2008; Phillips et al., 2004; Kundu et a., 2014). The convergence rate along the Leh-Ladakh region, around KF, is 17.8±1mm/yr., while the Western Himalaya and Garhwal-Kumaun Himalaya of the Central Himalaya reveal a lower convergence rate of ~15mm/yr. (Verma and Bansal, 2012; Jade et al., 2014, 2017; Mondal et al., 2016 and references therein). Besides KF, two major sinistral strike-slip faults are also located in southern Tibet, namely, (i) Longmu-Gozha Fault (LGF) and (ii) Karakax Fault (KXF) (Figure 3). South of these faults lies the KCR, a transverse and trans-tensional structure, which is suggested to have a seismogenic relationship to the earthquakes of the Garhwal Himalaya, located further south (Arora et al., 2012).

3. Stress Inversions

3.1. Data selection

The catalogue of FM solutions used in this study has been compiled from earlier studies and 86 solutions from the Global Centroid Moment Tensor (GCMT) catalogue (Baranowski et al., 1984; Chandra et al., 1974; Das Gupta et al., 1982; Dziewonski et al., 1981; Ekström et al., 2012; Gahalaut&Rao, 2009; Hazarika et al., 2017; Hajra et al., 2021; Kanna et al., 2018; Mahesh et al., 2018; Negi et al., 2017; Parija et al., 2018; Paul et al., 2018; Prasath et al., 2017; Ram et al., 2005; Rastogi, 1974; Singh et al., 2018; Srinagesh et al., 2018; Kumar et al., 2009; Molnar & Chen, 1983; Molar & Lyon-Caent, 1989; Srivastava et al., 1987; Tandon and Srivastava, 1975; Verma and Sekharm 1986;Verma et al., 2015; Yadav et al., 2016). Out of the available ~450 FM solutions, 376 solutions that passed the quality criteria were chosen for the detailed analysis. The primary role of the quality criteria was to select crustal earthquakes with magnitude M≥2.0. The majority of those earthquakes (N=334) are in the upper crust (0-25 km depth range). The quality criteria include (i) the technique used to obtain FM solutions (MT inverted results were given preference), (ii) availability of local network data, and (iii) minimal errors, e.g., DC% and CLVD% for MT solutions and number of available stations for other types of techniques such as FOCMEC, INVRAD. FOCMEC utilizes the onset of P-wave arrival (up and down motion) known as P-wave polarity readings (Snoke, 2003), while the INVRAD technique makes use of both P-wave polarity readings and body wave amplitude matching (Ebel and Bonjer, 1990). Polarity readings tend to vary and largely depend on the azimuthal coverage of seismic record and number of stations, while the FM solutions obtained using MT techniques show much more stability. Hence, in the instance of multiple solutions with moment tensors against other types of FM solutions, the MT solutions were preferred (Supplementary table S1).

Most of the MT solutions used in the study are obtained using the multi-point-source representation and iterative deconvolution method, similar to the one explained by Kikuchi and Kanamori (1991) for teleseismic earthquakes. The latest inversion programs such as Isolated Asperities (ISOLA) and Kinematic waveform inversion tools (KIWI) were used to achieve the MT solutions (Sokos and Zahradník, 2008; Cesca and Heimann, 2013). Further, in case of multiple solutions with similar techniques (e.g., MT), only the solutions obtained using local networks and with a larger number of station records were used. For example, in the case of M_L 5.5 Dharamshala earthquake (1986), which has multiple solutions, we have chosen the one which is based on local network data and has better azimuthal coverage (Supplementary Table S1). The resultant catalogue, which is used in the present study for stress inversion, thus has 324 FM solutions (Figure 3, 4; Supplementary tables S2, S3)

3.2. Methodology

We used an iterative joint inversion technique to obtain stress and fault orientations, based on the inversion method of Michael (1984, 1987). This assumes that the trace of the stress tensor is to be zero and the stress tensor is normalized.

$$Tr(\tau) = \sigma_1 + \sigma_2 + \sigma_3 = 0 \quad \text{- (1)}$$

Michael's stress inversion employs expressions for normal and shear tractions on a fault σ_n and τ as follows,

$$\tau N_i = \tau_{kj} n_j \left(\delta_{jk} - n_i n_k\right) \text{ (Simplified)} \quad \text{- (2)}$$

where $\delta_{jk}$is Kronecker delta. Tis traction along a fault, n is fault normal and N is the unit direction vector of shear stress along a fault. Here, τ is normalised to be 1.

Eq. (2) in matrix form may written as:

$$At=s \quad \text{- (3)}$$

where s is the unit direction of slip vector and t is the vector of stress components, expressed as follows,

$$t = [\tau_{11}\tau_{12}\tau_{13}\tau_{22}\tau_{23}]^T \quad \text{- (4)}$$

A is the $3 * 5$ matrix calculated from fault normal n,

$$\begin{bmatrix} \boldsymbol{n_1(n_2^2 + 2n_3^2)} & \boldsymbol{n_2(-n_1^2 + n_3^2)} & \boldsymbol{n_3(-2n_1^2 - n_2^2)} \\ \boldsymbol{n_2(1 - 2n_1^2)} & \boldsymbol{n_1(1 - 2n_2^2)} & \boldsymbol{-2n_1n_2n_3} \\ \boldsymbol{n_3(1 - 2n_1^2)} & \boldsymbol{-2n_1n_2n_3} & \boldsymbol{n_1(1 - 2n_3^2)} \\ \boldsymbol{n_1(-n_2^2 + n_3^2)} & \boldsymbol{n_2(n_1^2 + 2n_3^2)} & \boldsymbol{n_3(-n_1^2 - 2n_2^2)} \\ \boldsymbol{-2n_1n_2n_3} & \boldsymbol{n_3(1 - 2n_2^2)} & \boldsymbol{n_2(1 - 2n_3^2)} \end{bmatrix} \quad \text{- (5)}$$

Using Eq. (5) for focal mechanisms of K earthquakes with known fault normal (n) and slip vectors(s), a system of 3 K linear equations for five unknown components of stress tensor could be obtained. Finally, the eq. (1) can be applied to solve the system using generalized linear inversion in the L2-norm (Prasath et al., 2017 and references therein).

$$t = A^{-g}S \quad \text{- (6)}$$

The traditional stress inversion methods usually use both the nodal planes of the FM solutions, because it is difficult to differentiate the fault plane and auxiliary plane. Michael's method (1984) produces a less accurate stress tensor, owing to the incorrect orientations of the fault planes.

The stress inversions were performed in MATLAB environment using the program STRESSINVERSE (Vavryčuk, 2014, available at https://www.ig.cas.cz/en/stress-inverse/). This program utilizes both the nodal planes of FM solutions and makes use of the Mohr-Coulomb failure criterion and fault instability analysis to identify the fault planes and better stress orientations (Scoltz, 2002; Vavryčuk et al., 2015 and references therein).

The Mohr-Coulomb failure criterion shows that the shear stress on an active fault must exceed a critical value τ_c for failure (rupture) to occur. This value is calculated from effective normal stress σ, cohesion C and fault friction μ using the following relationship.

$$\tau_c = C + \mu\,(\sigma_n - p) \quad \text{- (7)}$$

Here, the effective normal stress σ is given as $(\sigma_n - p)$, where σ_n is normal stress and p is pore pressure.

and,

$$\tau_c = C + \mu \geq 0 \quad \text{- (8)}$$

If the Mohr-Coulomb failure criterion is satisfied, then the fault becomes unstable and breaks (occurrence of an earthquake). Higher the shear stress difference, more the instability of a fault and hence susceptible to failure; this fault is called the "principal" fault (Vavryčuk, 2011). The principal fault is defined as a point wherethe Mohr-Coulomb failure criterion touches the Mohr's circle diagram (Figure 5).

The instability analysis can be performed with the nominal values of 0 to 1, where the maximum value being the maximum possibility to be ruptured (Vavryčuk et al., 2013). The fault instability *I* (of all fault orientation) can be defined using the following formula,

$$I = \frac{\tau - \mu(\sigma - \sigma_1)}{\tau_c - \mu(\sigma_c - \sigma_1)} \quad \text{- (9)}$$

where, σ_c and τ_c are the effective normal and shear stresses along the principal fault, while τ and σ are the effective normal and shear stress along a fault (Figure 5).

The quantity I is independent of absolute stress values, hence the fault instability can be evaluated just from friction and shape ratio. Eq. (9) has been simplified as follows. Detailed steps could be checked from Vavryčuk et al. (2015).

$$I = \frac{\tau - \mu(\sigma - 1)}{\mu + \sqrt{1+\mu^2}} \quad \text{- (10)}$$

$$\sigma = n_1^2 + (1 - 2\mathrm{R})n_2^2 - n_3^2 \quad \text{- (11)}$$

$$\mu = \sqrt{n_1^2 + (1-2\mathrm{R})^2 n_2^2 + n_3^2 - (n_1^2 + (1-2\mathrm{R})n_2^2 - n_3^2)^2} \quad \text{- (12)}$$

Here, n is the fault normal expressed in the coordinate system of the principal stress conditions. The quantity R is the shape ratio (hereafter, R-value), which is the stress ratio between the principal stress axes (σ_1- σ_3), using the following relation (Gephart & Forsyth, 1984).

$$R = {(\sigma 1 - \sigma 2)}\Big/{(\sigma 1 - \sigma 3)} \quad \text{- (13)}$$

The R-value varies between 0 and 1 and provides information on the relative contribution of principal stresses to the overall stress field. A low R-value represent the influence of $\sigma 2$, besides $\sigma 1$, while the high R-value suggest the role of dominant $\sigma 1$

An alternative stress ratio (ϕ**)** has also been given in Michael. (1984), as follows,

$$\phi = {(\sigma 2 - \sigma 3)}\Big/{(\sigma 1 - \sigma 3)} \quad \text{- (14)}$$

The study by Delvaux et al. (1995) have shown the variation in ϕ-value for varying stress regime and explained the stress magnitude using this ϕ-value. We have used the following relationship by solving Eq. (13) and Eq. (14) to convert the ϕ values into R-values to discuss the stress magnitude of the principal stresses in this study (Figure 6).

242 $$\phi = 1 - R \quad (15)$$

243 Initially, the stress inversion has been applied to the dataset in iterations using Michael's
244 method to solve the stress field, without the instability criterion. Later, this information was
245 used to derive instability using Eq. (10) in the second iteration and the iterations are
246 continuously performed until the solutions converge to an optimal value. The identified faults
247 were plotted on Mohr circle diagram to identify the optimal planes (hereafter principal FM
248 solutions).

249 The friction (μ) values generally vary between 0.4 and 0.8 (Vavryčuk, 2011), however,
250 the friction value of up to 1.0 has been reported in the Himalayan region by Chander and
251 Gahalaut (1995). Hence, in the context of the present study, the friction coefficient with range
252 0.4-1.0 was used for the stress inversion.

253 A refined methodology has been applied to the dataset of 376 FM solutions; that is to use
254 only the mainshocks to remove the possible internal stress perturbations in the data (Martínez-
255 Garzón et al., 2016). The declustering method given by Reasenberg (1985) has been used for the
256 ISC catalogue of earthquakes for the reporting period and resulted in 324 FM solutions for the
257 analysis. A total of 191 FM solutions (out of 324) are from MT inversion techniques, while the
258 remaining are from one or a combination of the following techniques, (i) Body-wave synthetic
259 matching, (ii) P-wave polarity readings and (iii) Amplitude inversions.

260 **3.3. Initial identification of zones**

261 The dataset was initially inverted to evaluate the overall state of stress in the western
262 IECZ (Inv. ID 1, N=324). Taking into consideration the spatial variability of faulting types of the
263 available FM solutions, we categorized the data into three sets, viz., (i) HSB with thrust type
264 FM solutions (Inv. ID 2, N=259), (ii) north of HSB (Karakoram-western Tibet) with strike-slip

and normal fault type (Inv. ID 3, N=56) and (iii) HFT and IGP region with normal fault type (Inv. ID 4, N=9). Further, based on the regional and local variations in geology and tectonics and the geographical proximity of available the FM solutions, the region has been divided into a total of nine different zones (Inv. IDs 5-13, Table 1). Zones (1-4) are in the Himalayan Arc and includes Garhwal-Kumaun Himalaya (GKH), Shimla Hills (SH), Kangra-Chamba (KC) and Kishtwar-Zanskar (KZ). The Garhwal and Kumaun sectors have similar geological and tectonic setup and traditionally considered an integral part (Valdiya, 1980a, b), hence, these two regions have been considered as a single zone (GKH). The SH and the KC are different in many aspects such as geology, tectonics, and seismicity level, etc. Besides, the width of the LH is less in KC, compared to that of GKH and SH zones. Also, the seismic activity is high in the KC and GKH, when compared to the SH zone. Therefore, studying the stress pattern of these regions separately attain importance. The seismicity in KZ zone is mainly concentrated around the Kishtwar window and studied separately for stress inversion. HSZ, which is the epicentral region of the Kashmir earthquake, is spatially separated from rest of the zones (1-4) by the Kashmir basin, which produces very low seismicity; hence this zone is studied separately. Other than these zones, the earthquakes with predominantly normal faulting mechanisms in and around the NPS zone are assigned a separate zone (6). The zones (7) and (8) both are located around the KF in its north (KF-N) and central (KF-C) parts, separated by the Nubra valley, where no or little seismic activity is reported at present. Zone (9) is the only zone in the present study, which is focused completely on a transverse structure, i.e., KCR. The nine seismotectonic zones identified in this study are, (i) GKH with 145 FM solutions (Inv. ID 5), (ii) SH with 12 FM solutions (Inv. ID 6), (iii) KC with 47 FM solutions (Inv. ID 7), (iv) KZ with 24 FM solutions (Inv. ID 8), (v) HSZ with 37 FM solutions (Inv. ID 9), (vi) NPS with 9 FM solutions (Inv. ID 10), (vii) KF (north) with 13

FM solutions (Inv. ID 11), (viii) KF (central) with 10 FM solutions (Inv. ID 12) and (ix) KCR with 20 FM solutions (Inv. ID 13) (Figure 3 and 4). Besides, the inversion has been performed separately for the aftershocks of the Kashmir earthquake to understand its stress pattern from 37 FM solutions (Inv. ID 14, Supplementary table S4). For each inversion, we compute the best-fitting stress field vectors, maximum (σ1), intermediate (σ2) and minimum (σ3), the shape ratio/stress ratio (R-value), and principal FM solutions, which govern the susceptibility of a fault to be ruptured under the given stress conditions. Based on the results and the methodology explained in Martínez-Garzón et al. (2016) and Abolfathian et al. (2019), some of these zones have been further merged (Inv. IDs 15-17) and re-analyzed for results on stress distribution. The merged zones are (i) GKH-SH zone (Inv. ID 15, N=157), (ii) KC-KZ zone (Inv. ID 16, N=71) and KF zone (Inv. ID 17, N=23).

4. Results

The results of inversion for individual zones and different combinations are presented in Table 1 and Figure 7. The result of the inversion for the overall region with 324 FM solutions (Inv. ID 1) shows a compressional tectonic regime with dominant σ_1 oriented towards NE-SW (213.67º/14.5º ±1.7º, azimuth/plunge with error) and R-value of 0.88±0.03. Further, inversions for the Himalayan and Tibetan regions show distinct thrust and strike-slip faulting mechanisms respectively. The Himalayan region show NE-SW trending σ_1 (220.84º/13.9º ±1.7º), while the Karakoram-Tibet region show NNE-SSW trending σ_1 (25.99º/4.2º ±88.9º). The mixed stress regime between strike-slip and normal fault makes it difficult to distinctly derive σ_1 and σ_2 for this inversion; hence the inversion resulted in large errors for these two stress axes. The stress ratios 0.76±0.02 and 0.07±0.27 for these two broad zones, viz., the Himalaya (Inv. ID 2) and

311 Karakoram-Tibet (Inv. ID 3), respectively are different and are discussed in a later section.
312 Further, the comprehensive analysis on stress inversion quality by Martínez-Garzón et al. (2016)
313 suggests a minimum number of 20 FM solutions to resolve a stress field for noise-free data.
314 Therefore, the results for the HFT-IGP zone with only 9 FM solutions (Inv. ID 4) are not
315 discussed in detail (Table 1).

316 The zone-wise results obtained show varying tectonic stress fields and orientations for
317 different zones as presented below.

318 **4.1. Himalayan region**

319 The inversion results for zones in the Himalaya (Inv. IDs 5-13) show a compressional
320 tectonic regime with horizontal and dominant σ1 oriented towards NNE-SSW to NE-SW. The
321 SH region (Inv. ID 6) with only 12 solutions has been merged with GKH (Inv. ID 5), because
322 both the inversion results show similar and dominant σ_1 (210.6/20.2 ±6.0 and
323 213.89º/8.85º±2.5, respectively) with high R-values, 0.82±0.12 and 0.73±0.05, respectively.
324 The result of this merged zone i.e., GKH-SH (Inv. ID 15) with 157 FM solutions shows pure
325 compression with horizontal σ_1 (213.32º/10.8 ±2.1) and σ_2 (112.85º/2.52º±4.9) and vertical σ_3
326 (19.8º/78.96º ±4.9) with high R-value (0.80±0.03). Although the stress regime is similar in
327 different parts of the Himalaya, the stress orientation, in particular, the σ1 for the KC and KZ
328 zones are different from the GKH. The σ_1 for these two zones (KC and KZ) are estimated to be
329 233.21/18 ±9.5 and 220.3/18.4 ±8.0 with R-values 0.7±0.13 and 0.90±0.18, respectively. As
330 the two zones show close results, we have merged these zones to form a single zone (Inv. ID
331 16) and the results show pure compression with horizontal σ_1 (226.06/21 ±4.6) and σ_2
332 (132.15/10 ±12) with vertical σ_3 (18.19/66.45 ±11.9), while the stress ratio is estimated to be
333 0.87±0.04.

4.2. Hazara and Nanga Parbat Syntaxial zones

The results for the HSZ (Inv. ID 9) and the separate inversion for the aftershocks of Kashmir earthquake occurred between 8th October 2005 and 28th of December 2005 with magnitudes $M_W \geq 4.7$ (Inv. ID 14), both show nearly similar stress field with horizontal σ_1 (212.85/14 ±11.8 and 216.38/13.2 ±4.7, respectively) and σ_2 (120.62/8.86 ±11.2 and 124.9/6.29 ±10.4, respectively) and vertical σ_3 (359.2/73.34 ±7.7 and 9.96/75.35 ±9.9, respectively). However, the R-value varies significantly, 0.39±0.09 and 0.66±0.07 for HSZ (Inv. ID 9) and aftershocks of the Kashmir earthquake (Inv. ID 14) respectively. The NPS zone (Inv. ID 10) located to the northeast of the HSZ shows pure extension with vertical σ_1 (352.87/83.7 ±16.5) and horizontal σ_2 (237.12/2.75 ±16.9) and σ_3 (146.9/5.67 ±11.8) with R-value of 0.56±0.25. Even though the FM solutions available for this region (NPS zone) is few (N=9), with distinct fault type (normal) and for their peculiar location (within the NPS zone), these events are reported and discussed in the present study Besides, the errors are relatively low, hence the results are used for the discussion in the next section.

4.3. Karakoram-Tibet

Three zones have been identified in this region: two along the KF, in its north (Inv. ID 11) and its central segment (Inv. ID 12) and one along the transverse structure, KCR (Inv. ID 13). The results of the two zones along the KF are similar and have a low number of FM solutions (13 and 10, respectively), hence these two zones are merged to form a single zone (Inv. ID 17). The resultant inversion for the KF zone shows strike-slip motion with horizontal σ_1 (119.5/15.3 ±4.7), σ_3 (292.4/10.62 ±7.7) and vertical σ_2 (55.93/71.2 ±8.8) with an R-value of 0.79±0.09. The stress field for inversion of FM solutions along the transverse structure KCR (Inv. ID 13) shows that the region has a dominant strike-slip stress regime with horizontal σ_3

(262.8°/15.8° ±18.3°), sub-vertical σ_2 (154.88°/47.5° ±70.9°) and sub-vertical σ_1 (5.71°/38.2° ±70.9°) with very low R-value of 0.14±0.15.

The principal FM solutions (for the faults plotted on the upper and lower hemisphere of the Mohr's circle diagram, respectively) for each inversion have been presented in table (1) alongside the preliminary results.

5. Discussion: varying stress field and stress ratio

The computed stress field shows an overall transpressional stress regime with dominant σ_1 (Inv. ID 1). However, the individual zones often show quite different stress fields. The stress field for the events along the HSB (Inv. ID 2) shows compression with horizontal NE-SW-oriented σ_1, which is oblique to the direction of the on-going India-Eurasia collision (NNE-SSW). The high-stress ratio (R=0.88) suggests the dominant role of σ_1 in this terrane. Further, the low angle plunge for the σ_1(13.9 º), which suggests the mid-crustal ramp of the detachment (MHT) could be the causative fault in this stress regime. Moreover, the second nodal plane of the principal FM solution which corresponds to the individual faults projected on to the Mohr's circle diagram with 8.83º dip angle show conclusively that the shallow dipping detachment with 5°-10° dip angle is the causative fault and the most susceptible one for failure in the future (Seeber et al., 1981; Ni and Barazangi, 1984). The results for the Karakoram-Tibet regions (Inv. ID 3) show a transtensional stress regime with NNE-SSW-oriented σ_1 and a very low-stress ratio (R=0.07). The steep dip angles (90º and 85º) obtained from the principal FM solutions are consistent with the dominant strike-slip and transverse structures in this region, such as KF and KCR. In a strike-slip stress regime, the low value of R indicates dominant stress magnitudes of

σ_1 and a significant contribution from σ_2 (Figure 6 and 7). This suggests the influence of local structures along with the regional tectonic forces in the Karakoram-Tibet region.

5.1. The Himalayan region

The GKH-SH zone (Inv. ID 15) of the Central Himalaya shows compressional stress regime with arc-normal σ1 (NNE-SSW), i.e., perpendicular to the trend of Himalayan Arc, in good agreement with the direction of relative motion of the Indian plate with respect to the Eurasian plate (Figure 7 and 8). The high R-value of 0.80 indicates that the generation of seismogenic stress in the region is mainly controlled by σ1 (Table 1). The low-angle plunge of σ1 (10.8º) with the preferred nodal plane of principal mechanism (12.87º) suggest active deformation along the mid-crustal ramp of detachment, which has a shallow dip angle of <20º in this region (Ni & Barazangi, 1984; Caldwell et al., 2013 and references therein). Despite having similar (compressional) stress regimes such as the GKH-SH zone, the KC-KZ zone (Inv. ID 16) show arc-oblique principal compressive stress (i.e., oblique [$\sigma_1 \neq 90º$] to the structures of the Himalayan Arc; ~65º in this context) in comparison to the arc-normal principal compressive stress (σ1=90º to the Arc) for GKH-SH zone (Inv. ID 15) (Figure 7 and 8). Similarly, the plunge angle is also higher for this region (21º) in comparison to the GKH-SH zone (10.8º). However, the R-values and principal FM solutions are nearly similar for both zones. Previous studies based on the erosional rates, thermo-chronology, topography, geomorphological indicators, and earthquake MT solutions have proposed that the 77º E longitude, which separates the GKH-SH regions from the KC-KZ region, is a transition between contradictory tectonic settings on either side (Eugster et al., 2018; Nennewitz et al., 2018). Besides, Seeber & Pêcher (1998) proposed that the India-Eurasia convergence is arc-normal in the central Himalaya and becomes arc-oblique in western Himalaya, which is consistent with the recent plate motion models by Kundu

et al. (2014), where GPS slip vectors supports the arc-normal convergence in Central Himalaya (including GKH-SH zone) and oblique convergence in Western Himalaya (KC-KZ and Kashmir). In their study (Kundu et al., 2014), the obliquity of convergence angle in the central Himalaya marked as "obliquity 0" and the change in the obliquity for the western Himalaya reported to be ~29º±5º, which is comparable with the present study with change in the obliquity of ~14º between central Himalaya (Inv. ID 15) and western Himalaya (Inv. ID 16). It is to be noted that the obliquity changes from east to west as the KC zone shows obliquity of ~10º, while the KZ zone shows obliquity of around ~23º, consistent with the obliquity of ~29º±5 reported by Kundu et al. (2014). The oblique convergence along western Himalaya produces pure shear along the KF, located northeast of this region and thrusting along the Himalayan intra-crustal thrusts (Kundu et al., 2014 and references therein). The change in convergence perturbs the regional stress field and produces the arc-oblique stress field in the zones.

5.2 Hazara and Nanga Parbat syntaxes

The inversion for the declustered catalogue of FM solutions for the HSZ (Inv. ID 9) shows compression with principal stress axes like the ones for the GKH-SH zone (Inv. ID 15). The low R-value (0.39) for this zone suggests that the region experiences pure to radial compressional fault motion and indicate the significant contribution of σ_2, besides the dominant σ_1. This is probably due to the multiple tectonic forces present in the HSZ such as Hind Kush in the northwest, Pamir in the north and northeast and Himalaya in the southeast. Besides, unlike the study by Kundu et al. (2014), which suggests the HSZ has an oblique convergence like the KC-KZ zone, our study reports the stress field of the HSZ to be similar to the Central Himalaya with horizontal σ_1 (212.85/14 and 213.32º/10.8, respectively), σ_2 (120.62/8.86 and 112.85º/2.52º, respectively) and vertical σ_3 (359.2/73.34 and 19.8º/78.96º, respectively). The

NPS located northeast of the HSZ show pure extension with an R-value of 0.56. Despite the low number of available FM solutions, owing to similar faulting mechanisms in the zone (i.e., extension), the resultant stress field has acceptable errors ranging from 11.8° to 16.9° for principal stress axes and ±0.25 for R-value. The inversion result (pure extension) for this region (NPS, Inv. ID 10), which is located between the Kohistan and Ladakh batholiths, rules out the association of MMT in generation of seismicity in this region. Moreover, the principal FM solutions show the causative fault to have an extensional motion with a steep dip angle (~60º), further suggesting that the stress regime is controlled by normal faulting along the Kohistan batholith as proposed in the previous studies (DiPietro et al., 2000; Seeber & Pêcher, 1998. Moderate R-value (0.56) suggests pure extensional motion along the faults in this region, in contrast to the HSZ, with dominant σ_1 and minimal role of σ_2 and σ_3.

5.2.1 Aftershocks of 2005 Kashmir earthquake

The inversions for the Kashmir earthquake and its aftershocks show little difference in stress orientations from its epicentral region, i.e., HSZ (Figure 7). However, the stress ratio reveals a moderately high R-value (0.66) for the aftershock sequence (Inv. ID 14) than the inversion results of the declustered catalogue for its epicentral region (Inv. ID 9) (Table 1). This suggests the dominant role of σ_1 as in other Himalayan regions (e.g., GKH-SH and KC-KZ) during the Kashmir earthquake. However, the Hindu Kush and Pamir regions located adjacent to HSZ, show contrasting stress fields with the HSZ. The stress orientations for the 2005 aftershock sequence and its epicentral region (HSZ), show NNE-SSW oriented $\sigma_{1,}$ while the Hindu Kush and Pamir regions show NNW-SSE oriented strike-slip tectonics (Figure 7, 8) with varying stress orientation (σ_1) owing to different tectonic forces acting in these regions, such as slab pull in Hindu Kush region (Gahalaut & Rao, 2009 and references therein). Besides, the

KC-KZ zone (NE-SW oriented σ_1) separated from the HSZ by the Kashmir valley with very low seismicity also shows dissimilarity. In an earlier study, the stress field of the aftershocks of the Kashmir earthquake and HSZ were compared with that of the Himalaya, leading to apprehension over its origin being a Himalayan earthquake (Gahalaut & Rao, 2009). However, in their study, they used FM solutions of earthquakes from the entire Himalayan Arc. Besides, with more FM solutions and detailed zone wise analysis in the present study provides new insight into the stress field of the epicentral region of the Kashmir earthquake (HZS, Inv. ID 9) as well as its aftershocks (Inv. ID 14). The stress orientations for the HSZ and aftershock sequence shows horizontal σ_1 (212°/14° and 216°/13°), σ_2 (120/9° and 125/6°) and vertical σ_3 (359/73° and 10/55°), and the principal FM solutions are found to be similar to that of the Himalayan zones, e.g., for GKH-SH of the Central Himalaya region with σ_1=210°/17.5°, σ_2=118°/6° and σ_3 =8.9°/71°. Besides, the preferred fault planes from principal FM solutions for HSZ and the aftershock sequence of the Kashmir earthquake, show shallow dip angles (22º for both the inversions), similar to the mid-crustal ramp of the Himalaya (≤25º) (Table 1) (Gahalaut & Kalpna, 2001; Prasath et al., 2017; Seeber et al., 1981). Further, the moderately high R-value (0.66) for the aftershock sequence reveals nearly pure compression with dominant σ1 during the aftershock activity similar to the zones from the Himalayan Arc. Hence, we categorize the Kashmir earthquake to be a Himalayan-type earthquake.

5.3 Karakoram Fault

The seismicity around KF is concentrated in its north (approx. 37º-35º N) but diffused in the central zone (approx. 35º-33º N) separated by the aseismic Nubra valley (Figure 2). We performed the inversions separately for these two zones to understand the stress distribution

along the north and central segment of this fault. However, due to the unavailability of the required minimum number of FM solutions (N~20) for this region, the zones were merged. Besides, the area to the south of 33° N show almost negligible seismicity and could not be considered for the inversions. The results for the north and central segment of the KF show strike-slip tectonics with NE-SW oriented σ1, similar to that of the Himalayan region and suggestthe active nature of the KF. The high R-value (0.79) computed for the KF with strike-slip stress regime suggests transpressional motion (Figure 8 and 9). The geological study carried out by Raterman et al. (2007) on varying faulting style along the KF has reported transpressional motion along its northern segment between 37º and 34º N and transtension in its south between 34º and 32º N. In the present study, however, we could reliably determine a single stress field for the northern segments between 37° and 34° N, precisely up to 33.5° N (Inv. ID 17) with transpressional motion, which is well consistent with the geological and GPS velocity vectors (Raterman et al., 2007; Kundu et al., 2014). Also, the principal FM solutions for this zone suggest steeply dipping seismogenic fault with 74º-86º dip angle. Owing to the unavailability of FM solutions, the stress field for the southern segment of KF could not be attempted.

5.4 Kaurik Chango Rift

The stress field along the KCR shows that the region is currently experiencing mixed or oblique-slip tectonics with horizontal σ_3 and N-S oriented vertical σ_1 and σ_2, which is compatible with that of current geological, seismological and plate motion models, suggesting that the KCR region is experiencing E-W directed transtension (DiPietro et al., 2000; Gahalaut and Kundu., 2012; Jade et al., 2014; Tapponnier et al., 1981; Kundu et al., 2014). Besides, the very low R-value (0.15) indicates that the region is experiencing pure transtensional fault motion (Figure 9). The nodal planes of the principal FM solution obtained for the stress

494 inversion of earthquakes in this zone show steep dip angles (83° and 55°). The preferred fault
495 plane with strike 17.21°, dip 83.02° and rake -137.92° fits perfectly for the earlier geological
496 studies for this region with transtensional and steep dip angle (~80) (Gupta and Kumar, 1975),
497 hence we suggest this fault to be most susceptible to failure in the KCR zone.

498

499 **6. Conclusions**

500 This study summarizes that the western IECZ is characterized by a heterogeneous stress
501 regime. This heterogeneity exists owing to the variability in India-Eurasia convergence, local
502 and regional structures, and multiple tectonic forces. The results show that the Himalayan
503 seismic belt has a compressional stress regime with dominant σ_1, while the Karakoram and
504 Tibet regions show strike-slip faulting with dominant σ_1, as well σ_2. The preferred focal
505 mechanism for the Himalayas shows that the detachment (MHT) is the most susceptible fault
506 to be ruptured in the future, while a steep fault is more susceptible to failure for the Karakoram
507 and Tibet areas. Zone-wise analysis of focal mechanism solutions provide new insights, viz.,
508 (i) Arc-normal compression in Garhwal-Kumaun-Shimla hills region and arc-oblique
509 compression in Kangra-Chamba-Kishtwar-Zanskar region consistent with the GPS velocity
510 vectors and regional geology and tectonics, (ii) Himalayan-type stress field for the aftershocks
511 of Kashmir earthquake (2005) and Hazara Syntaxis, (iii) pure extension at Nanga Parbat
512 Syntaxis, (iv) transpressional fault motion for the Karakoram fault and (v) transtensional stress
513 regime for the transverse Kaurik Chango rift, with N-S trending $\sigma 1$ and steep dip angle. The
514 new results presented in this study will be useful for the advanced simulation of geodynamic
515 stress field, understanding seismogensis and assessing seismic hazard in the region.

Acknowledgments

We thank the Secretary, Ministry of Earth Sciences, Govt. of India for his encouragement and support. Suggestions made by S. Roy significantly improved the manuscript. We acknowledge Vineet Gahalaut for suggestions at initial stage and Vaclav Vavryčuk for providing valuable comments on the work. We also thank Komal, Joyeeta, Ojaswita, Mayank, Medha and Dhamu for their help and support. The data used in this study are compiled from different sources, viz., ISC Catalog, Global CMT catalogue, published journal articles and it can be accessed collectively from the supplementary tables or their respective sources, as mentioned in the article. We are grateful to two anonymous reviewers for their constructive comments and suggestions, which significantly improved the manuscript. Data have been compiled from various published sources and are available through respective sources as mentioned in supplementary table (1) or collectively be accessed from supplementary table (3) and (4).

Competing Interests

The authors declare no competing interests.

References

1. Abolfathian, N., Martínez-Garzón, P. and Ben-Zion, Y., 2019. Spatiotemporal variations of stress and strain parameters in the San Jacinto fault zone. Pure and Applied Geophysics, 176(3), pp.1145-1168.
2. Arora, B. R., Bansal, B. K., Prajapati, S. K., Sutar, A. K., & Nayak, S. (2017). Seismotectonics and seismogenesis of Mw7. 8 Gorkha earthquake and its aftershocks. *Journal of Asian Earth Sciences*, *133*, 2-11.
3. Arora, B. R., Gahalaut, V. K., & Kumar, N. (2012). Structural control on along-strike variation in the seismicity of the northwest Himalaya. *Journal of Asian Earth Sciences*, *57*, 15-24.
4. Banerjee, P. and Bürgmann, R. (2002). Convergence across the northwest Himalaya from GPS measurements. Geophysical Research Letters, 29(13), 30-1.
5. Baranowski, J., Armbruster, J., Seeber, L., & Molnar, P. (1984). Focal depths and fault plane solutions of earthquakes and active tectonics of the Himalaya. *Journal of Geophysical Research: Solid Earth*, 89(B8), 6918-6928.
6. Bott, M.H.P. (1959). The mechanics of oblique slip faulting. *Geological magazine*, 96(2), 109-117.
7. Caldwell, W.B., Klemperer, S.L., Lawrence, J.F. and Rai, S.S. (2013). Characterizing the Main Himalayan Thrust in the Garhwal Himalaya, India with receiver function CCP stacking. *Earth and Planetary Science Letters*, 367, 15-27.
8. Cesca, S. and Heimann, S. (2013). A practical on moment tensor inversion using the Kiwi tools. In New Manual of Seismological Observatory Practice 2 (NMSOP-2), 1-24. DeutschesGeoForschungsZentrum GFZ.

9. Chander, R. and Gahalaut, V.K. (1995). A simulation of upper crustal stresses for great and moderate thrust earthquakes of the Himalaya. *Proceedings of the Indian Academy of Sciences-Earth and Planetary Sciences*, 104(1), 115-129.
10. Chandra, U. (1978). Seismicity, earthquake mechanisms and tectonics along the Himalayan mountain range and vicinity. Physics of the Earth and Planetary Interiors, 16(2), 109-131.
11. Chaudhury, H. M., Srivastava, H. N., & Rao, J. S. (1974). Seismotectonic investigations of the Himalayas. *Him. Geol*, 4, 481-491.
12. Coudurier-Curveur, A., Tapponnier, P., Okal, E., Van der Woerd, J., Kali, E., Choudhury, S., Baruah, S., Etchebes, M. and Karakaş, Ç. (2020). A composite rupture model for the great 1950 Assam earthquake across the cusp of the East Himalayan Syntaxis. *Earth and Planetary Science Letters*, 531, p.115928.
13. Das Gupta, A., Srivastava, H. N., &Basu, M. S. (1982). Source mechanism of earthquakes in Kangra–Chamba region of Himachal Pradesh, India. Bull. Ind. Soc. Earthq. Tech, 19, 102-116.
14. Das, S. and Filson, J.R. (1975). On the tectonics of Asia. *Earth and Planetary Science Letters*, 28(2), pp.241-253.
15. DiPietro, J. A., Hussain, A., Ahmad, I., & Khan, M. A. (2000). The Main Mantle Thrust in Pakistan: its character and extent. *Geological Society, London, Special Publications*, *170*(1), 375-393.
16. Dziewonski, A. M., Chou, T. A., & Woodhouse, J. H. (1981). Determination of earthquake source parameters from waveform data for studies of global and regional seismicity. *Journal of Geophysical Research: Solid Earth*, *86*(B4), 2825-2852.

17. Ebel, J.E. & Bonjer, K.P. (1990). Moment tensor inversion of small earthquakes in southwestern Germany for the fault plane solution. *Geophysical Journal International*, 101(1), 133-146.
18. Ekström, G., Nettles, M., & Dziewoński, A. M. (2012). The global CMT project 2004–2010: Centroid-moment tensors for 13,017 earthquakes. *Physics of the Earth and Planetary Interiors*, *200*, 1-9.
19. Eugster, P., Thiede, R. C., Scherler, D., Stübner, K., Sobel, E. R., & Strecker, M. R. (2018). Segmentation of the Main Himalayan Thrust Revealed by Low-Temperature Thermochronometry in the Western Indian Himalaya. *Tectonics*, *37*(8), 2710-2726.
20. Gahalaut, K. and Rao, N.P., 2009. Stress field in the western Himalaya with special reference to the 8 October 2005 Muzaffarabad earthquake. *Journal of seismology*, *13*(3), p.371.
21. Gahalaut, V. K., & Kalpna. (2001). Himalayan mid-crustal ramp. *Current Science*, 1641-1646.
22. Gahalaut, V. K., & Kundu, B. (2012). Possible influence of subducting ridges on the Himalayan arc and on the ruptures of great and major Himalayan earthquakes. *Gondwana Research*, *21*(4), 1080-1088.
23. Gephart, J. W., & Forsyth, D. W. (1984). An improved method for determining the regional stress tensor using earthquake focal mechanism data: application to the San Fernando earthquake sequence. *Journal of Geophysical Research: Solid Earth*, *89*(B11), 9305-9320.
24. Gansser, A. (1964). Geology of the Himalayas: London, Wiley Interscience, 289 pp.
25. Gupta, V.J. and Kumar, S. (1975). Geology of Ladakh, Lahaul and Spiti regions of Himalaya with special reference to the stratigraphic position of flysch deposits.

Geologische Rundschau (International Journal of Earth Sciences), 64(1), 540-563. https://doi.org/10.1007/BF01820682.

26. Hajra, S., Hazarika, D., Kumar, N., Pal, S.K. and Roy, P.N.S. (2021). Seismotectonics and stress perspective of the Kumaon Himalaya: A geophysical evidence of a Lesser Himalayan duplex. *Tectonophysics*, 806, p.228801.
27. Hazarika, D., Paul, A., Wadhawan, M., Kumar, N., Sen, K., & Pant, C. C. (2017). Seismotectonics of the Trans-Himalaya, Eastern Ladakh, India: Constraints from moment tensor solutions of local earthquake data. Tectonophysics, 698, 38-46.
28. Hintersberger, E., Thiede, R. C., Strecker, M. R., & Hacker, B. R. (2010). East-west extension in the NW Indian Himalaya. *Bulletin*, *122*(9-10), 1499-1515.
29. Ichikawa, M., Srivastava, H.N. and Drakopoulos, J. (1972). Focal mechanisms of earthquakes occurring in and around the Himalayan and Burmese mountain belts. *Pap. Meteorol. Geophys.(Tokyo)*, 23, pp.149-162.
30. ISC (2019). International Seismological Centre, online bulletin, http://www.isc.ac.uk ,Thatcham, United Kingdom.
31. Jade, S., Mukul, M., Gaur, V. K., Kumar, K., Shrungeshwar, T. S., Satyal, G. S., ... & Banerjee, S. (2014). Contemporary deformation in the Kashmir–Himachal, Garhwal and Kumaon Himalaya: significant insights from 1995–2008 GPS time series. *Journal of Geodesy*, *88*(6), 539-557.
32. Jade, S., Shrungeshwara, T. S., Kumar, K., Choudhury, P., Dumka, R. K., &Bhu, H. (2017). India plate angular velocity and contemporary deformation rates from continuous GPS measurements from 1996 to 2015. *Scientific reports*, *7*(1), 1-16.

627 33. Kanna, N., Gupta, S., & Prakasam, K. S. (2018). Micro-seismicity and seismotectonic
628 study in Western Himalaya–Ladakh-Karakoram using local broadband seismic data.
629 Tectonophysics, 726, 100-109.
630 34. Khan, P.K., Ansari, M.A. and Mohanty, S. (2014). Earthquake source characteristics along
631 the arcuate Himalayan belt: Geodynamic implications. *Journal of Earth System Science*,
632 123(5), 1013-1030.
633 35. Kumar, S. and Mahajan, A.K. (1991). Dharamsala seismotectonic zone–Neotectonic and
634 state of stress in the area. *Himalayan Geology*, 21, pp.53-57.
635 36. Kumar, N., Sharma, J., Arora, B. R., & Mukhopadhyay, S. (2009). Seismotectonic model
636 of the Kangra–Chamba sector of northwest Himalaya: Constraints from joint hypocenter
637 determination and focal mechanism. Bulletin of the Seismological Society of America,
638 99(1), 95-109.
639 37. Kumar, R., Gupta, S.C. and Kumar, A. (2015). Effect of azimuthal coverage of an
640 earthquake on moment tensor solutions estimated by waveform inversion. *Arabian*
641 *Journal of Geosciences*, 8(8), 5713-5726.
642 38. Kundu, B., Yadav, R. K., Bali, B. S., Chowdhury, S., &Gahalaut, V. K. (2014). Oblique
643 convergence and slip partitioning in the NW Himalaya: Implications from GPS
644 measurements. *Tectonics*, *33*(10), 2013-2024.
645 39. Leech, M. L. (2008). Does the Karakoram fault interrupt mid-crustal channel flow in the
646 western Himalaya?. *Earth and Planetary Science Letters*, *276*(3-4), 314-322.
647 40. Li, S., Wang, Q., Yang, S., Qiao, X., Nie, Z., Zou, R., ... & Chen, G. (2018). Geodetic
648 imaging mega-thrust coupling beneath the Himalaya. *Tectonophysics*, *747*, 225-238.

649 41. Mahesh, P., Gupta, S., Saikia, U. and Rai, S.S., 2015. Seismotectonics and crustal stress
650 field in the Kumaon–Garhwal Himalaya. *Tectonophysics*, *655*, pp.124-138.
651 42. Martínez-Garzón, P., Ben-Zion, Y., Abolfathian, N., Kwiatek, G. and Bohnhoff, M. (2016).
652 A refined methodology for stress inversions of earthquake focal mechanisms. *Journal of*
653 *Geophysical Research: Solid Earth*, 121(12), 8666-8687.
654 43. Michael, A.J. (1984). Determination of stress from slip data: faults and folds. *Journal*
655 *of Geophysical Research: Solid Earth*, 89(B13), 1517-11526.
656 44. Michael, A.J. (1987). Use of focal mechanisms to determine stress: a control study. *Journal*
657 *of Geophysical Research: Solid Earth, 92*(B1), 357-368.
658 45. Molnar, P., Fitch, T.J. and Wu, F.T. (1973). Fault plane solutions of shallow earthquakes
659 and contemporary tectonics in Asia. *Earth and Planetary Science Letters*, 19(2), 101-112.
660 46. Molnar, P., Chen, W. P., and Fitch, T. J. (1977). Structure and tectonics of the Himalaya:
661 a brief summary of relevant geophysical observations.
662 47. Molnar, P., & Chen, W. P. (1983). Focal depths and fault plane solutions of earthquakes
663 under the Tibetan plateau. Journal of Geophysical Research: Solid Earth, 88(B2), 1180-
664 1196.
665 48. Molnar, P., & Lyon-Caent, H. (1989). Fault plane solutions of earthquakes and active
666 tectonics of the Tibetan Plateau and its margins. Geophysical Journal International, 99(1),
667 123-153.
668 49. Molnar, P. and Tapponnier, P. (1978). Active tectonics of Tibet. Journal of Geophysical
669 Research: Solid Earth, 83(B11), 5361-5375.

50. Mondal, S. K., Borghi, A., Roy, P. N. S., & Aoudia, A. (2016). GPS, scaling exponent and past seismicity for seismic hazard assessment in Garhwal–Kumaun, Himalayan region. *Natural Hazards*, *80*(2), 1349-1367.
51. Nennewitz, M., Thiede, R. C., & Bookhagen, B. (2018). Fault activity, tectonic segmentation, and deformation pattern of the western Himalaya on Ma timescales inferred from landscape morphology. *Lithosphere*, *10*(5), 632-640.
52. Negi, S. S., Paul, A., Cesca, S., Kriegerowski, M., Mahesh, P., & Gupta, S. (2017). Crustal velocity structure and earthquake processes of Garhwal-Kumaun Himalaya: Constraints from regional waveform inversion and array beam modeling. Tectonophysics, 712, 45-63.
53. Ni, J., & Barazangi, M. (1984). Seismotectonics of the Himalayan collision zone: Geometry of the underthrusting Indian plate beneath the Himalaya. *Journal of Geophysical Research: Solid Earth*, *89*(B2), 1147-1163.
54. Parija, M. P., Kumar, S., Tiwari, V. M., Rao, N. P., Kumar, N., Biswal, S., & Singh, I. (2018). Microseismicity, tectonics and seismic potential in the Western Himalayan segment, NW Himalaya, India. Journal of Asian Earth Sciences, 159, 1-16.
55. Paul, H., Priestley, K., Powali, D., Sharma, S., Mitra, S., & Wanchoo, S. (2018). Signatures of the existence of frontal and lateral ramp structures near the Kishtwar Window of the Jammu and Kashmir Himalaya: evidence from microseismicity and source mechanisms. Geochemistry, Geophysics, Geosystems, 19(9), 3097-3114.
56. Phillips, R. J., Parrish, R. R., & Searle, M. P. (2004). Age constraints on ductile deformation and long-term slip rates along the Karakoram fault zone, Ladakh. *Earth and Planetary Science Letters*, *226*(3-4), 305-319.

57. Prasath, R. A., Paul, A., & Singh, S. (2017). Upper crustal stress and seismotectonics of the Garhwal Himalaya using small-to-moderate earthquakes: Implications to the local structures and free fluids. *Journal of Asian Earth Sciences*, *135*, 198-211.
58. Prasath, R.A., Paul, A. and Singh, S. (2019). Earthquakes in the Garhwal Himalaya of the Central seismic gap: A study of historical and present seismicity and their implications to the seismotectonics. *Pure and Applied Geophysics*, *176(11)*, 4661-4685.
59. Ram, V. S., Kumar, D., &Khattri, K. N. (2005). The 1986 Dharamsala earthquake of Himachal Himalaya–estimates of source parameters, average intrinsic attenuation and site amplification functions. *Journal of seismology*, *9*(4), 473-485.
60. Raterman, N.S., Cowgill, E. and Lin, D. (2007). Variable structural style along the Karakoram fault explained using triple-junction analysis of intersecting faults. *Geosphere*, 3(2), 71-85.
61. Reasenberg, P. (1985). Second-order moment of central California seismicity, 1969-1982. *Journal of Geophysical Research: Solid Earth*, 90(B7), 5479-5495.
62. Seeber, L., & Pêcher, A. (1998). Strain partitioning along the Himalayan arc and the Nanga Parbat antiform. *Geology*, *26*(9), 791-794.
63. Seeber, L., Armbruster, J. G., & Quittmeyer, R. C. (1981). Seismicity and continental subduction in the Himalayan arc. *Zagros Hindu Kush Himalaya Geodynamic Evolution*, *3*, 215-242.
64. Singh, D.D. and Gupta, H.K. (1980). Source dynamics of two great earthquakes of the Indian subcontinent: The Bihar-Nepal earthquake of January 15, 1934 and the Quetta earthquake of May 30, 1935. *Bulletin of the Seismological Society of America*, 70(3), 757-773.

715 65. Singh, R., Prasath, R. A., Paul, A., & Kumar, N. (2018). Earthquake swarm of Himachal
716 Pradesh in northwest Himalaya and its seismotectonic implications. Physics of the Earth
717 and Planetary Interiors, 275, 44-55.
718 66. Snoke, J.A., (2003). FOCMEC: Focal mechanism determinations. International Handbook
719 of Earthquake and Engineering Seismology, 85, 1629-1630.
720 67. Sokos, E.N. and Zahradnik, J. (2008). ISOLA a Fortran code and a Matlab GUI to perform
721 multiple-point source inversion of seismic data. *Computers & Geosciences*, 34(8), 967-
722 977.
723 68. Srinagesh, D., Singh, S. K., Suresh, G., Srinivas, D., Pérez-Campos, X., & Suresh, G.
724 (2018). A study of Guptkashi, Uttarakhand earthquake of 6 February 2017 (M w 5.3) in
725 the Himalayan arc and implications for ground motion estimation. Journal of Seismology,
726 22(3), 789-803.
727 69. Srivastava, P. and Mitra, G. (1994). Thrust geometries and deep structure of the outer and
728 lesser Himalaya, Kumaon and Garhwal (India): Implications for evolution of the
729 Himalayan fold-and-thrust belt. *Tectonics*, 13(1), 89-109.
730 70. Tandon, A.N. (1972). Anantnag earthquakes (February–April 1967). *Ind. J. Meteor.*
731 *Geophys*, 23, pp.491-502.
732 71. Tandon, A. N., & Srivastava, H. N. (1975). Focal mechanisms of some recent Himalayan
733 earthquakes and regional plate tectonics. Bulletin of the Seismological Society of America,
734 65(4), 963-969.
735 72. Tapponnier, P., Mercier, J.L., Armijo, R., Tonglin, H. and Ji, Z., 1981. Field evidence for
736 active normal faulting in Tibet. *Nature*, *294*(5840), pp.410-414.

73. Thakur, V. C. (1992). Geology of western Himalaya. *Physics and Chemistry of the Earth*, *19*, 1-355.

74. Thakur, V. C., & Jayangondaperumal, R. (2015). Seismogenic active fault zone between 2005 Kashmir and 1905 Kangra earthquake meizoseismal regions and earthquake hazard in eastern Kashmir seismic gap. *Current Science (00113891)*, *109*(3).

75. Vavryčuk, V. (2011). Principal earthquakes: Theory and observations from the 2008 West Bohemia swarm. *Earth and Planetary Science Letters*, 305(3-4), 290-296.

76. Vavryčuk, V., 2014. Iterative joint inversion for stress and fault orientations from focal mechanisms. *Geophysical Journal International*, *199*(1), pp.69-77.

77. Vavryčuk, V., Beer, M., Kougioumtzoglou, I., Patelli, E. and Au, I.K. (2015). Earthquake mechanisms and stress field. *Encyclopedia of earthquake engineering*, 728-746.

78. Vavryčuk, V., Bouchaala, F. and Fischer, T. (2013). High-resolution fault image from accurate locations and focal mechanisms of the 2008 swarm earthquakes in West Bohemia, Czech Republic. *Tectonophysics*, 590, 189-195.

79. Verma, M. and Bansal, B.K. (2012). Indian National GNSS Programme: crustal deformation measurements in the Indian Sub-continent. *Journal of Asian Earth Sciences*, 50, 1-6.

80. Verma, M. and Bansal, B.K. (2013). Seismic hazard assessment and mitigation in India: an overview. *International Journal of Earth Sciences*, 102(5), 1203-1218.

81. Verma, R. K., & Sekhar, C. C. (1986). Focal mechanism solutions and nature of plate movements in Pakistan. Journal of geodynamics, 5(3-4), 331-351.

82. Verma, R.K., Mukhopadhyay, M. and Roy, B.N. (1977). Seismotectonics of the Himalaya, and the continental plate convergence. *Tectonophysics*, 42(2-4), pp.319-335.

83. Verma, M., Sutar, A. K., Bansal, B. K., Arora, B. R., & Bhat, G. M. (2015). MW 4.9 earthquake of 21 August, 2014 in Kangra region, Northwest Himalaya: Seismotectonics implications. *Journal of Asian Earth Sciences*, *109*, 29-37.
84. Wallace, R.E. (1951). Geometry of shearing stress and relation to faulting. *The Journal of geology*, 59(2), 118-130.
85. Wallis, D., & Searle, M. P. (2019). Spatial and Temporal Distributions of Deformation in Strike-Slip Faults: The Karakoram Fault in the India-Asia Collision Zone. In *Transform Plate Boundaries and Fracture Zones* (pp. 271-300). Elsevier.
86. Yadav, D. K., Hazarika, D., & Kumar, N. (2016). Seismicity and stress inversion study in the Kangra–Chamba region of north-west Himalaya. *Natural Hazards*, *82*(2), 1393-1409.
87. Yadav, D. K., Kumar, N., Hazarika, D., Yadav, D. N., & Wadhawan, M. (2017). Seismicity and Tectonics of Kinnaur Himalaya and adjoining region inferred from focal mechanism solutions and stress tensor inversion. *Himalayan Geology*, *38*(1), 49-55.

Author Contributions

R.A.P., B.K.B., and M.V. have conceived the research problem. R.A.P. performed data compilation and analysis. R.A.P., B.K.B., and M.V. interpreted the results. R.A.P. drafted the figures and All the authors contributed in finalizing the manuscript.

Figure captions

Figure 1. Structure, tectonics and earthquakes of the Himalaya. The filled stars are epicenters of historical earthquakes with magnitudes ≥ 7.6. The study area, i.e., western India-Eurasia collision zone is marked by a rectangle with solid lines. Figure modified from Prasath et al. (2019). FM solutions are taken from GCMT catalogue and published records (Coudurier-Curveur et al., 2020; Singh and Gupta, 1980).

Figure 2. The western India-Eurasia Collision Zone, its structure, tectonics and seismicity. (a) Study area including major geological structures and tectonic elements (Thakur, 1992; Thakur & Jayamgondaperumal, 2005; Wallis & Searle, 2019). Acronyms: AK-Almora Klippen, BBF-Balakot Bagh Fault, HFT-Himalayan Frontal Thrust, HHC-Higher Himalayan Crystallines, HS-Hazara Syntaxis, IGP-Indo Gangetic Plains, ITS-Indus Tsangpo Suture, JF-Jhelum Fault, KB-Kashmir Basin, KCR-Kaurik Chango Rift, KF-Karakoram Fault, KLRW-Kullu-Larji-Rampur Window, KW-Kishtwar Window, KXF-Karakax Fault, LGF-Longmu Gozha Fault, LH-Lesser Himalaya, MBT-Main Boundary Thrust, MCT-Main Central Thrust, MKT-Main Karakoram Thrust, MMT-Main Mantle Thrust, NPS-Nanga Parbat Syntaxis, SH-Sub Himalaya, SRT-Salt Range Thrust, STD-Southern Tibetan Detachment, TH-Tethyan Himalaya, TP-Tibetan Plateau. Landmark locations: CA-Chamba, DD-Dehradun, IS-Islamabad, JU-Jammu, KA-Kangra, KL-Kargil, LE-Leh, MB-Muzaffarabad, NI-Ngari, SA-Shimla, SI-Spiti and SN-Srinagar.

Figure 3. Earthquakes used in the present study. Epicenters of FM solutions used in the present study with the background seismicity retrieved from the International Seismological Center (ISC). The seismotectonic zones are marked with dotted lines, viz., (1) Garhwal-Kumaun Himalaya (GKH), (2) Shimla Hills (SH), (3) Kangra-Chamba zone (KCZ), (4)

Kishtwar-Zanskar (KZ), (5) Hazara Syntaxial zone (HSZ), (6) Nanga Parbat Syntaxis (NPS), (7) Northwest Karakoram Fault (KF-N), (8) Southeast Karakoram Fault (KF-S) and (9) Kaurik Chango Rift (KCR). Acronyms are similar to those given in Fig. 2.

Figure 4. Earthquake Focal Mechanism solutions used in the present study. The figure shows the Earthquake FM solutions. Acronyms are similar to those given in Fig. 2 and Fig. 3.

Figure 5. Mohr-Coulomb failure criterion and Instability analysis. (a) All possible orientations of fault planes that satisfy the Mohr–Coulomb failure criterion has been shown in darken area in orange color. The optimally oriented principal fault planes with respect to stress are shown in blue square dots, while the C refers to the cohesion. Upper and lower half of the planes correspond to conjugate faults. (b) The tractions on the principal fault characterized by instability I = 1 is marked by red filled polygon. The tractions of an arbitrarily oriented fault with instability I is shown in black dot.

Figure 6. Stress ratio, stress magnitude and stress regimes. Relationship between stress ratio, stress magnitude and stress regime for the Inversion IDs 1-17, representing the different seismotectonic zones (see Fig. 2).

Figure 7. Stress inversion plots of the present study. (a) Principal stress and P/T axes, (b) Confidence of the stress axes, (c) Mohr circle diagram and (d) Shape ratio 'R'.

Figure 8. Principal stress axes from the stress inversions plotted with the respective zones. Stress fields for 2005 Kashmir earthquake and its aftershocks, Hindukush and Pamir are taken from Gahalaut and Rao (2009). Structure and tectonic features are similar to Fig. 2.

Figure 9. Salient conclusion of the work. Schematic diagram showing the major results such as sense of fault motion, stress regime and principal stress direction in the western India-Eurasia collision zone.

Table(s)

Table 1. Results of stress inversions using earthquake focal mechanisms in the western IECZ.

*Az-Azimuth, Pl-Plunge, S1/S2-Strike 1 and 2, D1/D2-Dip 1 and 2, R1/R2-Rake 1 and 2, R-Shape ratio and μ-Friction Coefficient. *5-8, 11 and 12 are used for discussion.**Errors are common for both Azimuth and Plunge values*

Supplementary Table 1: List of FM solutions with multiple sources.

** At appropriate place: the reason for choosing the final solution has been mentioned.*

Supplementary Table 2: Sources used in the present study for preliminary data

Supplementary Table 3: All data preliminary locations

Supplementary Table 4: FM solutions used in this study

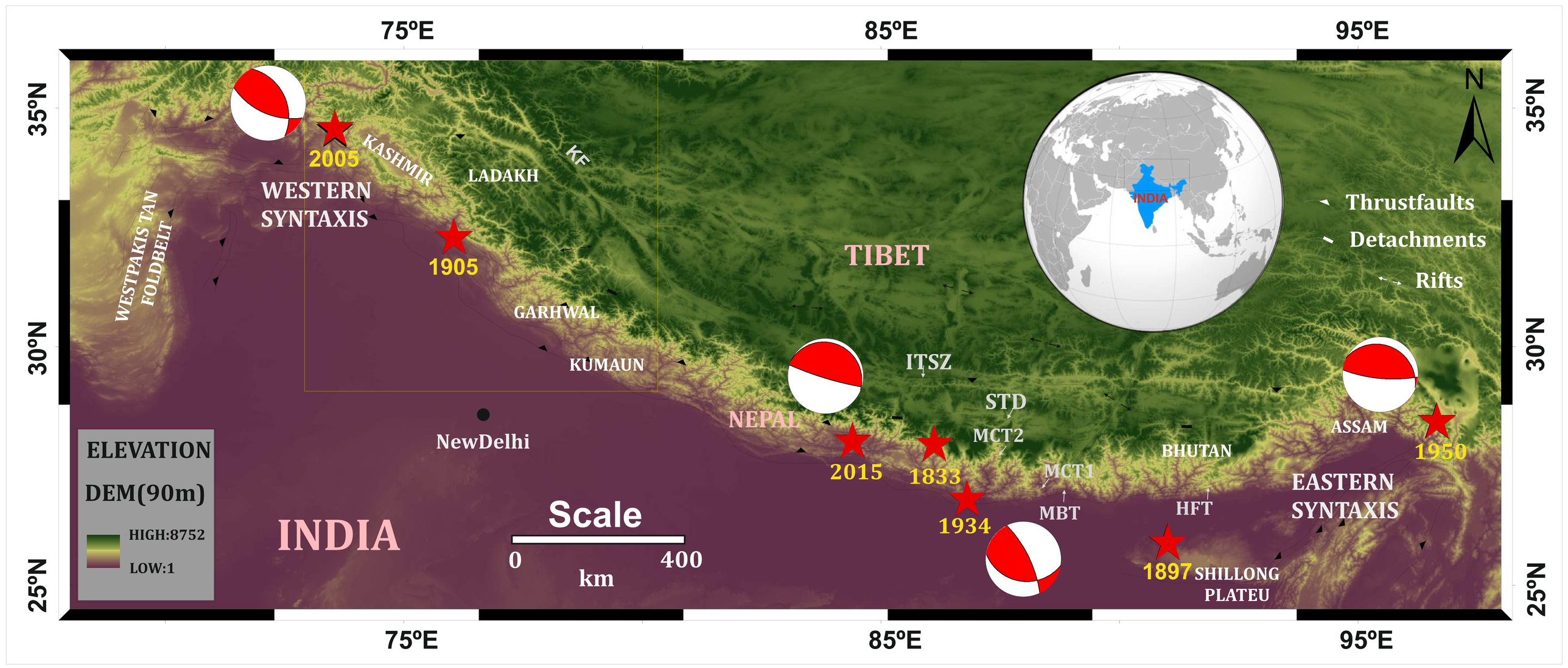
75ºE
85ºE
95ºE
35ºN
30ºN
25ºN
N
Thrustfaults
Detachments
Rifts
INDIA
TIBET
2005
KASHMIR
LADAKH
KF
WESTERN
SYNTAXIS
WESTPAKIS TAN
FOLDBELT
1905
GARHWAL
KUMAUN
NewDelhi
ITSZ
STD
MCT2
NEPAL
2015
1833
MCT1
MBT
1934
BHUTAN
HFT
ASSAM
1950
EASTERN
SYNTAXIS
1897
SHILLONG
PLATEU
ELEVATION
DEM(90m)
HIGH:8752
LOW:1
INDIA
Scale
0
400
km

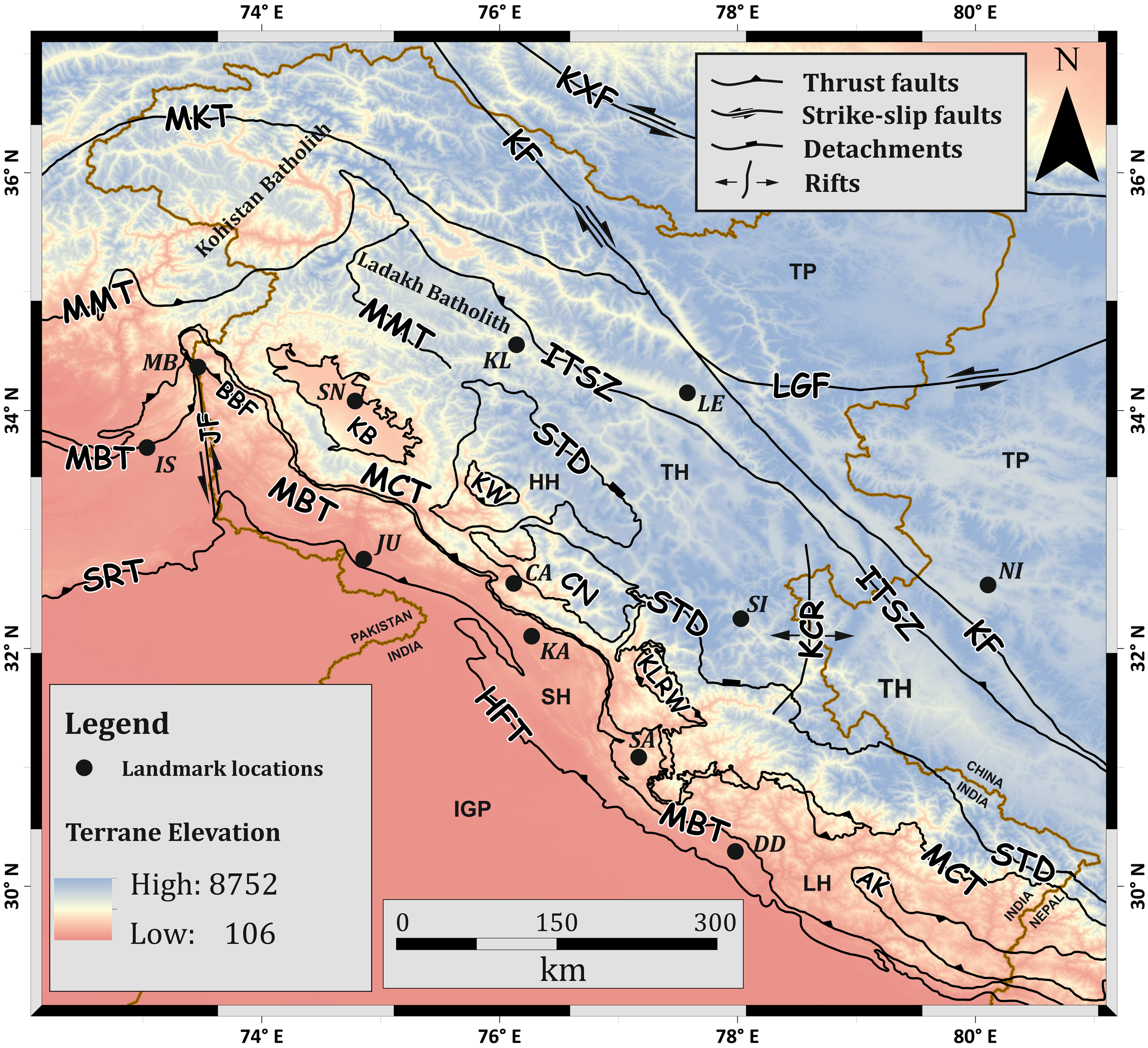
74° E
76° E
78° E
80° E
36° N
34° N
32° N
30° N
N
Thrust faults
Strike-slip faults
Detachments
Rifts
MKT
Kohistan Batholith
KXF
KF
MMT
Ladakh Batholith
MMT
ITSZ
LGF
MB
KL
LE
BBF
SN
KB
JF
STD
MBT
IS
MCT
KW
HH
TH
TP
MBT
JU
SRT
CA
CN
STD
SI
KCR
ITSZ
KF
NI
PAKISTAN
INDIA
KA
KLRW
SH
HFT
TH
SA
CHINA
INDIA
IGP
MBT
DD
MCT
STD
LH
AK
INDIA
NEPAL
Legend
Landmark locations
Terrane Elevation
High: 8752
Low: 106
0
150
300
km

74° E
76° E
78° E
80° E
36° N
34° N
32° N
30° N
N
HSZ
NPS
KF-N
KF
KF-C
KCR
KZ
KC
SH
GKH
MB
IS
SN
KL
LE
JU
CA
KA
SI
NI
SA
DD
Legend
Final catalogue (N=324)
Landmark locations
ISC catalogue
Magnitude scale
1.5 - 3.9
4.0 - 5.9
6.0 - 7.6
0
125
250
km

74° E
76° E
78° E
80° E
36° N
34° N
32° N
30° N
N
NPS
KF
KZ
KCZ
KCR
HSZ
SH
GKH
MB
IS
JU
SN
KL
LE
SI
SA
DD
NI
Magnitude scale
M 2.0
M 3.0
M 4.0
M 5.0
M 6.0
M 7.0
M 7.6
FM types
Thrust / Reverse
Normal / Gravity
Strike-slip
Legend
Final catalogue (N=324)
Landmark locations
0
125
250
km

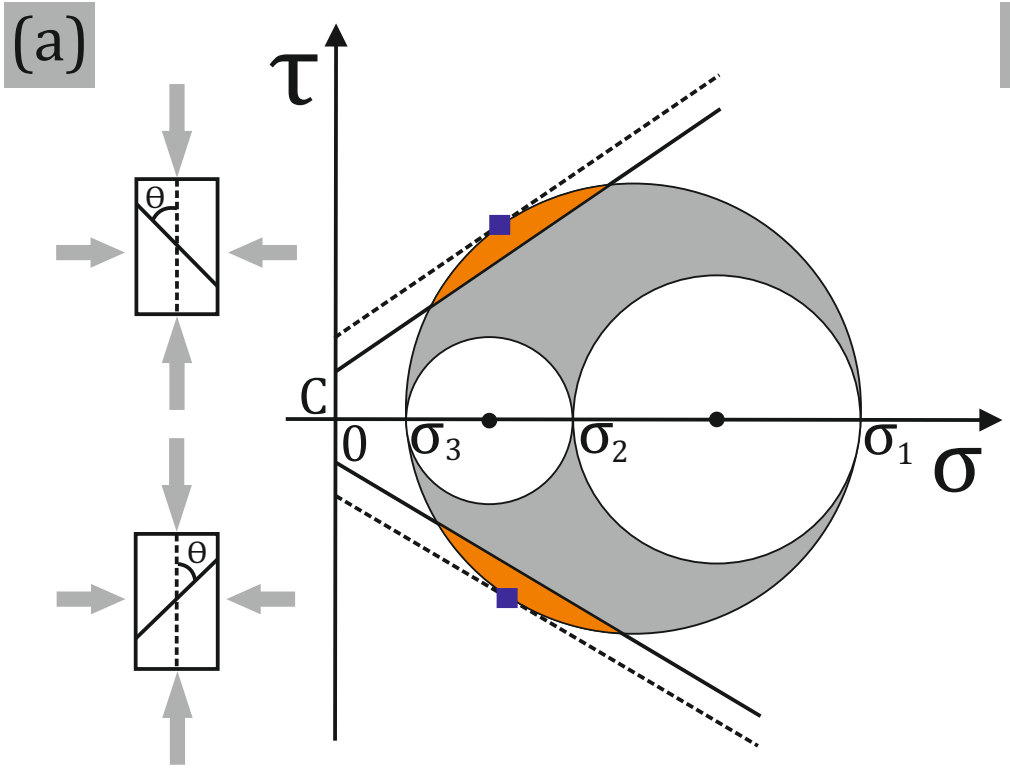

Mohr-Coulomb Failure Criterion

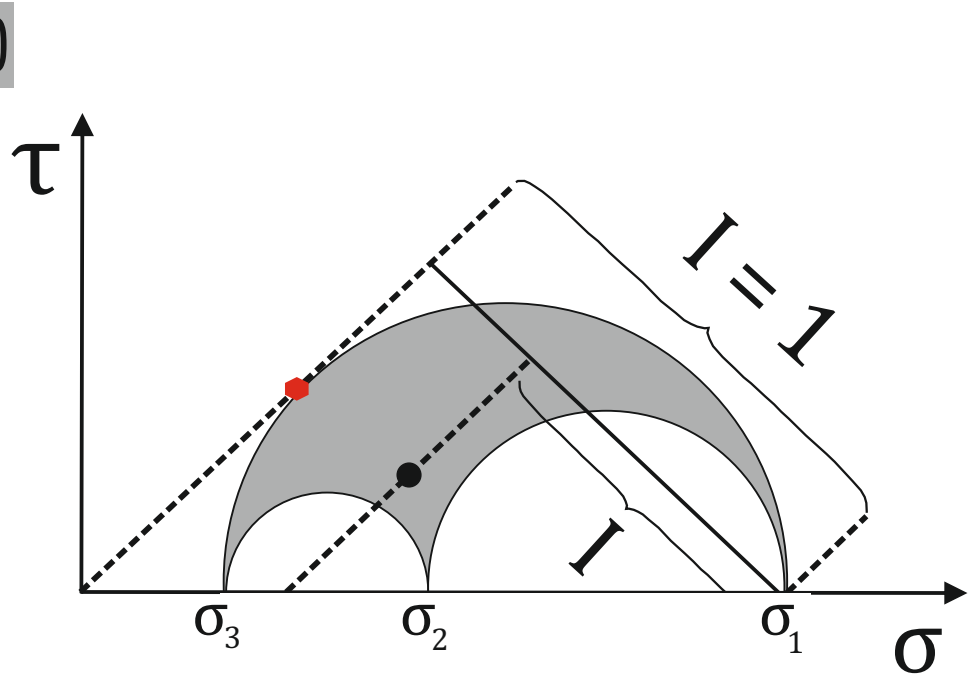

Fault Instability

Stress Regimes	Types				
Extensive	**Radial** 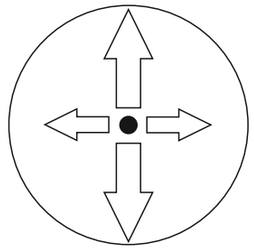 R=0.9; φ=0.1	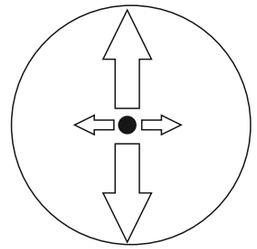 R=0.7; φ=0.3	**Pure** 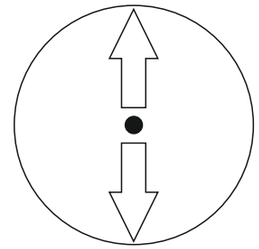 R=0.5; φ=0.5	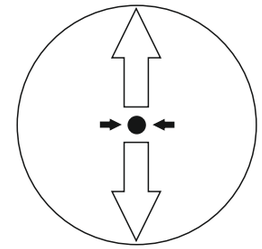 R=0.3; φ=0.7	**Strike-slip** 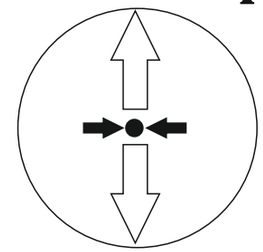 R=0.1; φ=0.9
Strike-slip	**Extensive** 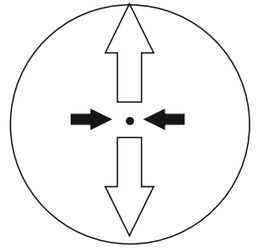 R=0.1; φ=0.9	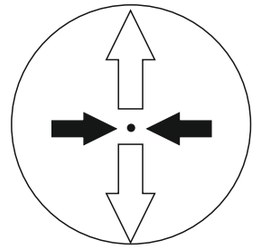 R=0.3; φ=0.7	**Pure** 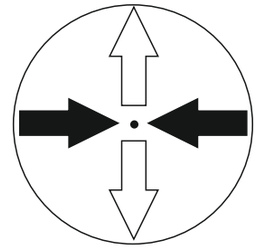 R=0.5; φ=0.5	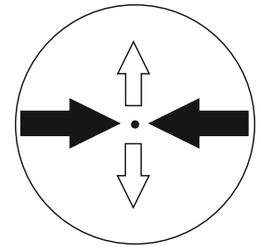 R=0.7; φ=0.3	**Compressive** 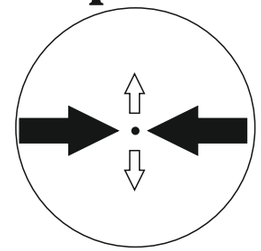 R=0.9; φ=0.1
Compressive	**Strike-slip** 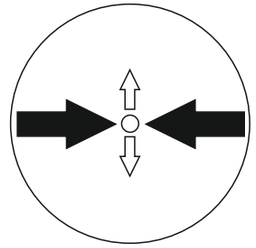 R=0.9; φ=0.1	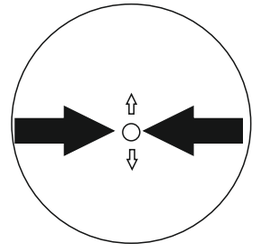 R=0.7; φ=0.3	**Pure** 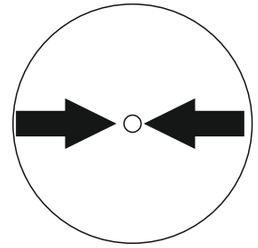 R=0.5; φ=0.5	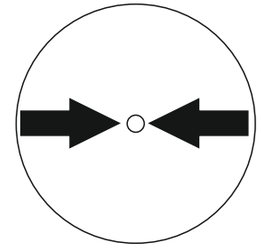 R=0.3; φ=0.7	**Radial** 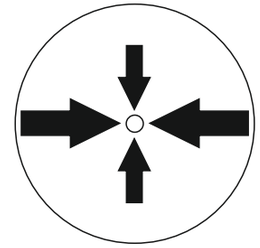 R=0.1; φ=0.9

(a) (b) (c) (d)

INV. ID 1 INV. ID 2 INV. ID 3 INV. ID 4 INV. ID 5 INV. ID 6 INV. ID 7 INV. ID 8 INV. ID 9 INV. ID 10

(a) (b) (c) (d)

INV. ID 11 INV. ID 12 INV. ID 13 INV. ID 14 INV. ID 15 INV. ID 16 INV. ID 17

(a) Principle stress and P/T axes

Sigma 1
Sigma 2
Sigma 3

(b) Confidence of principle stress axes

Sigma 1
Sigma 2
Sigma 3

(c) Mohr circle diagram

(d) Shape ratio / Stress ratio

74° E
76° E
78° E
80° E
36° N
34° N
32° N
30° N
N
NPS
KF
HSZ
KC+KZ
KCR
GKH-SH
0
125
250
km
Legend
GPS vectors
(Kundu et al., 2014)
(i)
(ii)
(iii)
Terrane Elevation
High: 8614
Low: 106
Horizontal Stress
Sigma 1
Sigma 2
Sigma 3
Vertical Stress
Sigma 1
Sigma 2
Sigma 3

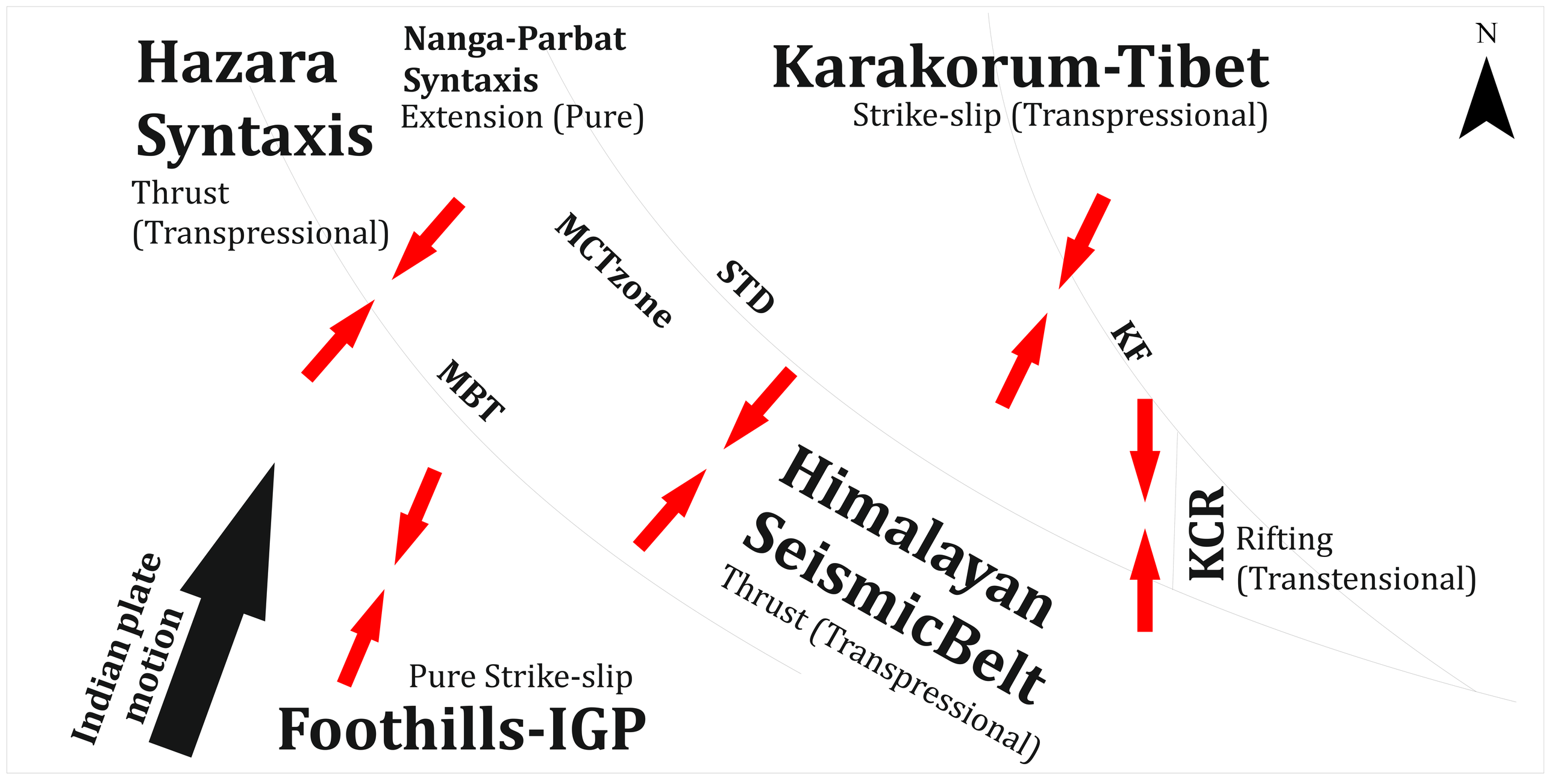
Hazara Syntaxis
Thrust (Transpressional)
Nanga-Parbat Syntaxis
Extension (Pure)
Karakorum-Tibet
Strike-slip (Transpressional)
N
MCTzone
STD
KF
MBT
Himalayan SeismicBelt
Thrust (Transpressional)
KCR
Rifting (Transtensional)
Indian plate motion
Pure Strike-slip
Foothills-IGP

Table 1a

Inversion ID (Inv. ID)*	Area	FM solutions used	Sigma 1 (Degrees)			Sigma 2 (Degrees)			Sigma 3 (Degrees)		
			Az	Pl	Err**	Az	Pl	Err	Az	Pl	Err
1	Whole dataset (declustered)	324	213.67	14.47	01.7	122.8	3.4	06.5	19.88	75.12	06.5
2	Himalayan Seismic Belt	259	220.84	13.94	01.7	129.73	4.47	03.0	22.34	75.33	03.1
3	Karakorum-Tibet	56	25.99	4.2	88.9	171.51	84.91	88.9	295.78	2.87	03.3
4	HFT & IGP regions	9	202.18	19.93	25.8	78.6	56.75	69.8	302.1	25.44	71.1
5	Garhwal-Kumaun Himalaya	145	213.89	8.85	02.5	123.74	0.99	4.68	27.38	81.10	4.35
6	Shimla Hills	12	210.6	20.34	06.0	57.26	67.47	24.0	304.07	9.28	23.3
7	Kangra-Chamba	47	233.21	18.01	09.5	135.11	23.43	34.7	357.1	59.75	34.6
8	Kishtwar-Zanskar	24	220.3	18.39	08.0	128.97	3.99	17.9	27.17	71.15	17.9
9	Hazara Syntaxial zone	37	212.85	14	11.8	120.62	8.86	11.2	359.24	73.34	07.7
10	Nanga Parbat Syntaxial zone	9	352.87	83.69	16.5	237.12	2.75	16.9	146.85	5.67	11.8
11	Karkorum Fault (north)	13	204.15	41.42	37.6	72.41	37.04	56.9	320.28	26.52	46.3
12	Karakorum Fault (south)	10	28.21	4.66	14.9	125.33	56.66	21.9	295.18	32.93	21.8
13	Kauric Chango Rift	20	5.71	38.24	70.9	154.88	47.46	70.9	262.83	15.8	18.3
14	Aftershocks of 2005 Kashmir EQ	37	216.38	13.2	04.7	124.9	6.29	10.4	9.96	75.35	09.9
15	Inv. IDs 5+6	157	213.32	10.75	02.1	122.85	2.52	04.9	19.8	78.96	04.9
16	Zone IDs 7+8	71	226.06	21.01	04.6	132.15	10.03	12.0	18.19	66.45	11.9
17	Zone IDs 11+12	23	199.5	15.29	04.7	55.93	71.24	08.8	292.44	10.62	07.7

Table 1b

Inversion ID (Inv. ID)*	Principle mechanisms						R	Pie	Error	Friction Coefficient	Sense of motion
	Upper Hemisphere			Lower Hemisphere							
	S1	D1	R1	S2	D2	R2					
1	118.32	37.27	84.39	325.27	8.83	112.72	0.88	0.12	0.03	0.99	Transpression
2	124.10	38.37	82.78	333.20	11.11	113.87	0.76	0.24	0.02	0.89	Pure Compression to Transpression
3	351.79	89.97	174.92	59.91	85.23	-1.87	0.07	0.93	0.27	0.40	Transtension
4	56.51	76.15	30.53	3.76	57.68	-171.76	0.48	0.52	0.49	0.80	NA
5	122.26	33.85	88.22	307.17	16.17	93.57	0.73	0.27	0.03	0.84	
6	55.88	89.43	22.52	11.27	73.39	-164.57	0.82	0.18	0.12	0.94	
7	111.42	47.18	57.16	38.01	23.59	173.56	0.70	0.30	0.13	1.00	
8	124.89	44.42	84.29	337.12	8.41	118.42	0.90	0.10	0.18	0.79	
9	112.80	48.88	78.20	323.64	21.74	114.57	0.39	0.61	0.09	0.40	Radial to Pure compression
10	58.51	63.30	-86.92	234.97	51.96	-93.49	0.56	0.44	0.25	0.47	Pure Extension
11	65.59	81.06	52.43	29.77	48.10	-144.04	0.77	0.23	0.61	0.98	NA
12	359.60	61.89	161.28	51.94	57.77	9.04	0.81	0.19	0.08	1.00	

13	147.21	83.02	-137.92	24.40	55.08	-26.03	0.14	0.86	0.15	0.40	Transtension
14	119.14	47.67	81.48	320.95	21.73	107.21	0.66	0.34	0.07	0.40	Pure Compression
15	119.13	34.23	85.51	313.96	12.87	101.39	0.80	0.20	0.03	0.94	Pure Compression to Transpression
16	121.89	44.82	75.69	35.93	10.10	173.88	0.87	0.13	0.04	1.00	Pure Compression to Transpression
17	44.12	86.03	18.35	359.92	74.27	-169.64	0.79	0.21	0.09	1.00	Pure Compression to Transpression